ADVANCED ENERGY MATERIALS

Supporting Information

for *Adv. Energy Mater.,* DOI: 10.1002/aenm.201600660

Quaternary Organic Solar Cells Enhanced by Cocrystalline Squaraines with Power Conversion Efficiencies >10%

Tenghooi Goh, Jing-Shun Huang, Kevin G. Yager, Matthew Y. Sfeir, Chang-Yong Nam, Xiao Tong, Louise M. Guard, Patrick R. Melvin, Francisco Antonio, Benjamin G. Bartolome, Minjoo L. Lee, Nilay Hazari, and André D. Taylor**

Quaternary Organic Solar Cells Enhanced by Co-crystalline Squaraines with Power Conversion Efficiencies >10%

Tenghooi Goh[a,§], Jing-Shun Huang[1,5,§], Kevin G. Yager[2], Matthew Y. Sfeir[2], Chang-Yong Nam[2], Tong Xiao[2], Louise M. Guard[3], Patrick R. Melvin[3], Francisco Antonio[1], Benjamin Bartolome[1], Minjoo L. Lee[4], Nilay Hazari[3★], and André D. Taylor [1★]

Table of content

S1. Spectral overlap and Förster radius estimation of energy transfer pairs in the active layer

S1a. ASSQ emission and DPSQ absorption

S1b. ASSQ emission and PT8, PTB7, PTB7-Th absorption

S1c. PT8, PTB7 emission and DPSQ absorption

S1d. Estimation of FRET radii, measured in dilute solution of chlorobenzene

S1e. Photoluminescence (PL) of polymer-squaraine films

S2. TA time- and spatial resolved images of squaraines and PTB7-Th blends

S3. GIWAXS data

S3a GIWAXS: Ternary PTB7:$PC_{71}BM$ blends, (c) in-plane, and (d) out-of-plane line-cut

S3b. GIWAXS: PTB8:$PC_{61}BM$ (binary) and ASSQ:DPSQ:PT8:$PC_{61}BM$ (quarternary)

S3c. Summary of crystallite population in binary and quaternary PTB7:$PC_{71}BM$ systems

S3d. Fitting data of out-of-plane linecut of 1% ASSQ-DPSQ PTB7:$PC_{71}BM$

S3e. Summary of domain orientation percentage on binary, ternary, and quaternary films

S4. Hole mobility comparison for binary, ternary, and quaternary PTB7:$PC_{71}BM$ devices

S5. X-ray Photoelectron Spectroscopy (XPS):

[1]Department of Chemical and Environmental Engineering, Yale University, New Haven, CT 06511, USA
[2]Center for Functional Nanomaterials, Brookhaven National Laboratory, Upton, NY 11973, USA
[3]Department of Chemistry, Yale University, New Haven, CT 06520, USA
[4]Department of Electrical Engineering, Yale University, New Haven, CT 06511, USA
[5]Currently with Thomas J. Watson Laboratories of Applied Physics, California Institute of Technology, Pasadena, CA 91125, USA

[§]The authors equally contributed to the work.
★e-mail: andre.taylor@yale.edu; nilay.hazari@yale.edu

S5a. Surface element quantification of quaternary and binary PTB7:$PC_{71}BM$ films

S5b. N peak scans of quaternary PTB7:$PC_{71}BM$ film

S5c. N peak scans of ASSQ:DPSQ film

S6. Cross section SEM (X-SEM) and TEM with energy dispersive X-ray analysis (EDAX)

S6a. X-SEM of binary and quaternary cells on ITO (or glass portion of ITO substrates).

S6b-c EDAX and TEM images of quaternary films: Dual squaraines added (b) PTB7:$PC_{71}BM$ and (c) PT8:$PC_{61}BM$

S7 Solar cell IV and EQE of Ternary Solar Cells (2% wt. squaraine added)

S7a-b. J-V curves of (a) 2% ASSQ and (b) 2% DPSQ ternary PTB7:$PC_{71}BM$ under dark and 1sun illumination exposure

S7c-d. Photovoltaic parameter changes of (c) 2% ASSQ and (d) 2% DPSQ ternary PTB7:$PC_{71}BM$ cells under various radiation intensities from 0.1 to 1 sun

S7e-f. EQE difference obtained from figure S3c for (e) 2% ASSQ and (f) 2% DPSQ based PTB7:$PC_{71}BM$ based ternary solar cells.

S8 Solar cell performance of Quaternary Solar Cells using ZnO as interlayer:

S8a. PCEs of 60 devices of ASSQ:DPSQ:PTB7:$PC_{71}BM$ quaternary films under AM 1.5 1 Sun simulated illumination

S8b-d. Dark J-V curves of binary and quaternary of (b) PTB7:$PC_{71}BM$, (c) PTB7-Th:$PC_{71}BM$, and (d) PT8:$PC_{61}BM$ based solar cells cells

S8e-f. EQE difference between quaternary and binary (ΔEQE) of (e) PTB7:$PC_{71}BM$ based solar cells while the (f) EQE and ΔEQE of PTB7-Th:$PC_{71}BM$.

S9a Energy level alignment and device parameter statistics of quaternary systems.

S9a. PTB7:$PC_{71}BM$ with ASSQ and DPSQ

S9b. PTB7-Th:$PC_{71}BM$ with ASSQ and DPSQ

S9c. PT8:$PC_{61}BM$ with ASSQ and DPSQ

S9d. Statistics of device parameters with PFN as interlayer

S1. Spectral Overlap and estimation of Förster radius for energy transfer pairs

*****_The absorption spectra here are results from solution samples, as opposed to film samples in Fig. 1_

S1a. ASSQ emission and DPSQ absorption

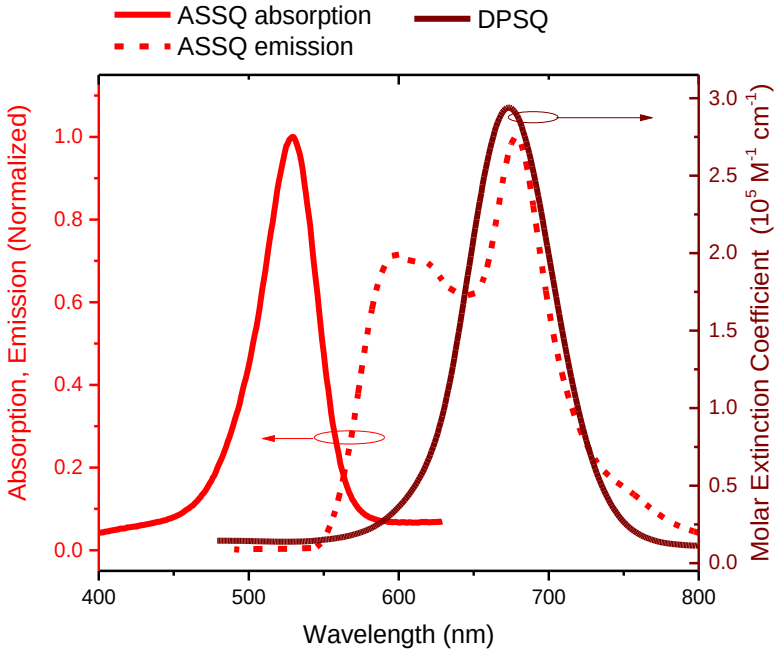

S1b. ASSQ emission and PT8, PTB7, PTB7-Th absorption

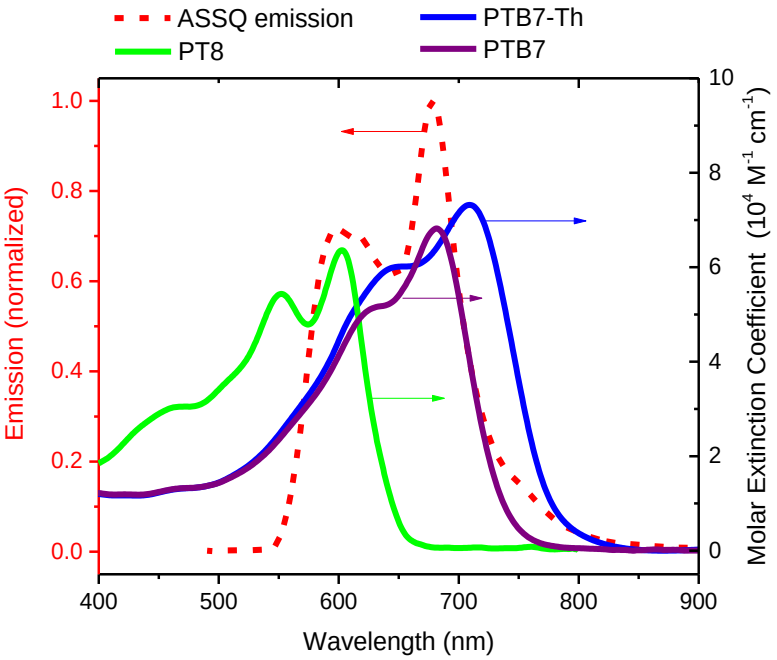

S1c. PT8, PTB7 emission and DPSQ absorption

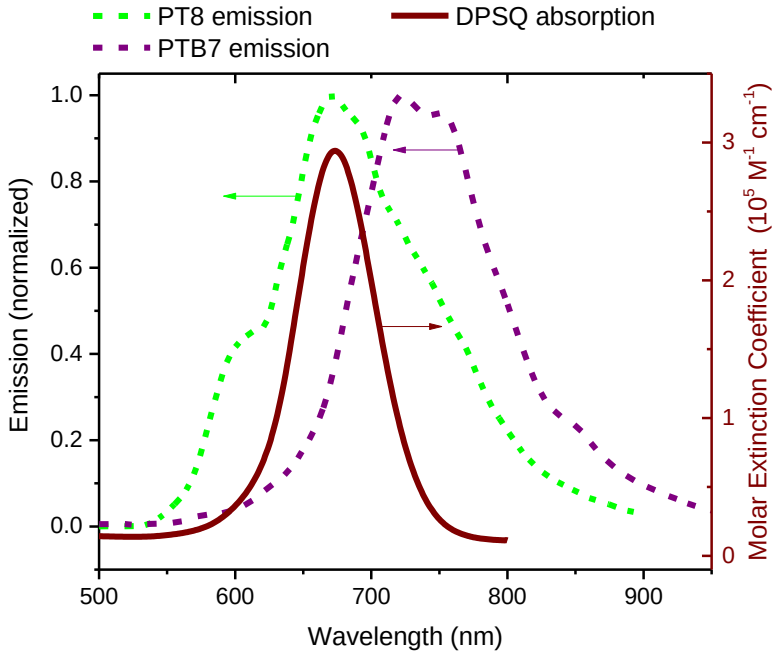

S1d. Estimation of FRET radii, measured in dilute solution of chlorobenzene

FRET Donor-Acceptor Pair	**Overlap Integral, *J(λ)*** ($M\text{-}1cm^3(nm)^4$)	***Q_D****	**R_0** (Å)
ASSQ→DPSQ	1.038×10^{16}	0.045	46.11
ASSQ→PTB7	5.657×10^{15}	0.045	41.68
ASSQ→PT8	6.192×10^{14}	0.045	28.82
PTB7→DPSQ	2.523×10^{15}	0.0097	28.81
PT8→DPSQ	2.195×10^{16}	0.126	62.03

*Quantum yield for ASSQ is determined by referencing to Rhodamine 610 (Q_R ~ 0.015 in ethanol); while Indocyanine green dye (IR 125), (Anal. Chem. **83** 1232 2011) (Q_R ~ 0.132 in ethanol; absorption at 633 nm) is used as reference for PTB7 and PT8 quantum yield calculation according to the following equation.

$$Q_D = Q_R \frac{\eta_D^{\,2}}{\eta_R^{\,2}} \frac{I_D}{A_D} \frac{A_R}{I_R} \qquad (1)$$

Q_D denotes the quantum yield of the donor (emitting) material; I represents the integrated fluorescence intensity; A refers the absorbance at excitation wavelength whereas the subscript R indicates the respective parameters of reference dye.

We quantified the compatibility of these FRET pairs by measuring the Förster radius, R_0, of the donor-acceptor separation distance where FRET is 50% efficient

$$R_0 = 9.78 \times 10^2 \left[\frac{\kappa^2 Q_D}{n^4} \int F_D(\lambda) \varepsilon_A(\lambda) \lambda^4 d\lambda \right]^{1/6} \text{(in nm)}, \qquad (2)$$

where κ is the orientation factor between donor and acceptor dipoles, Q_D is the quantum yield of FRET donor , n is the refractive index, F_D is the donor emission spectrum and ε_A is the molar extinction coefficient of the acceptor[1]. Assuming a random orientation of the donor and acceptor molecules (κ^2 = 2/3) and effective refractive index, n of 1.5 of these active materials in dilute solutions.

S1e. Photoluminescence (PL) of polymer-squaraine films

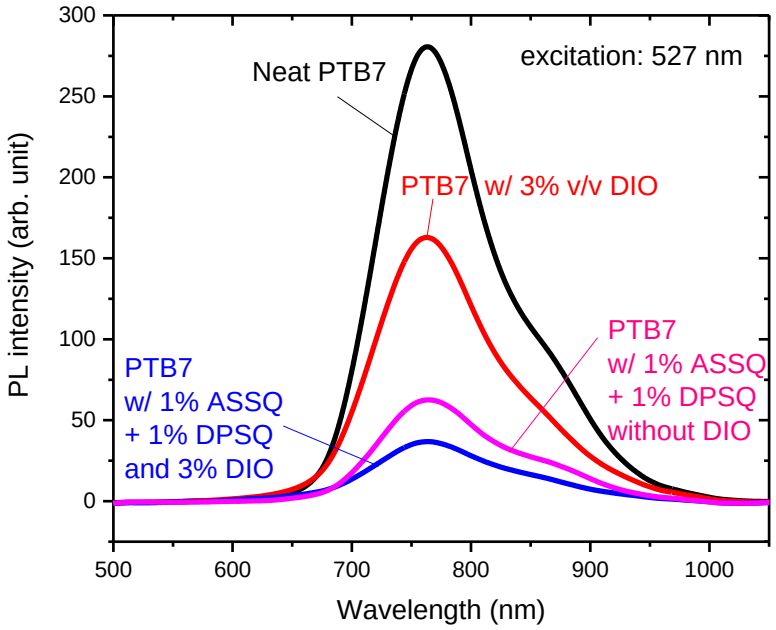

The PL quenching observed in squaraine-added samples indicate that the squaraines can effectively induce resonance energy transfer within the multi-donor films. The role of squaraines in the films differs from the 1,8-diiodooctane (DIO) additive as DIO does not participate in light absorption.

S2 Transient absorption time- and spatial resolved images for multi-donor blend in PTB7-Th system excited at 500 nm

(a) PTB7-Th

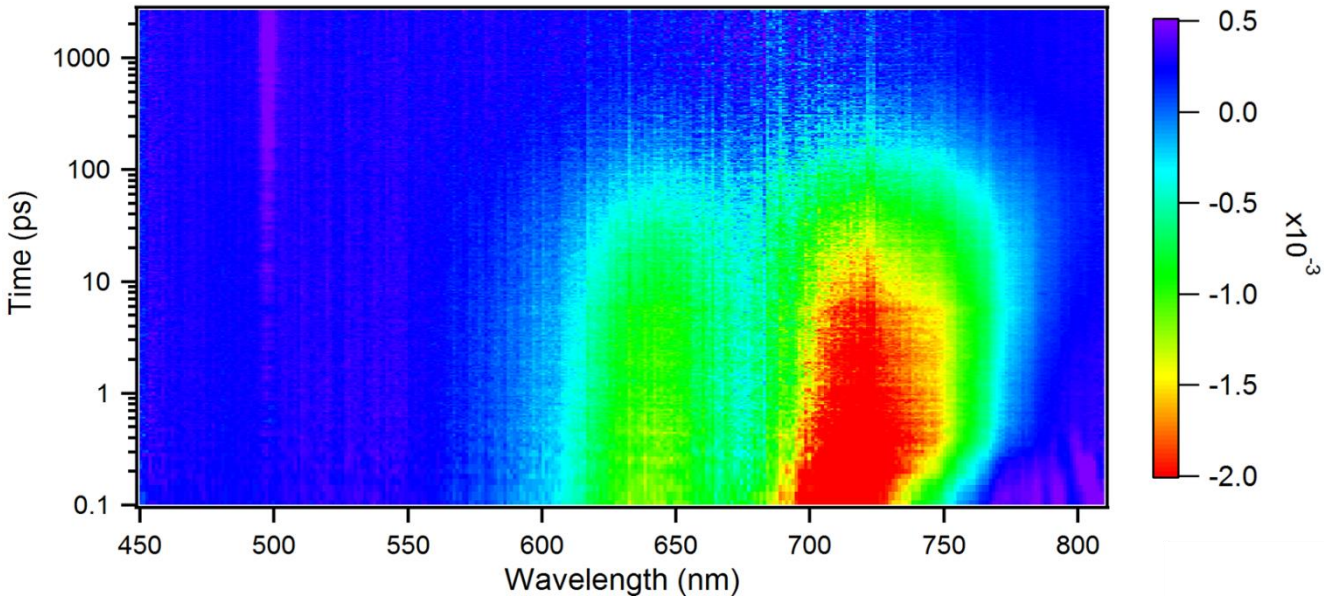

(b) PTB7-Th with 2% ASSQ

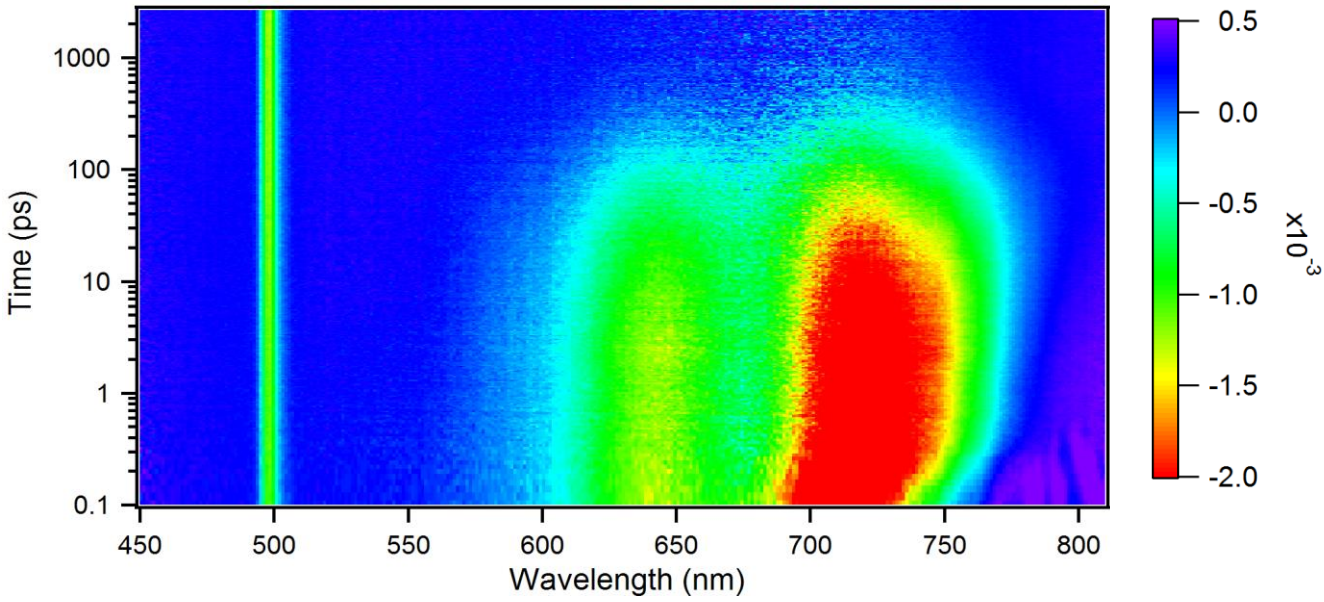

(c) PTB7-Th with 2% DPSQ

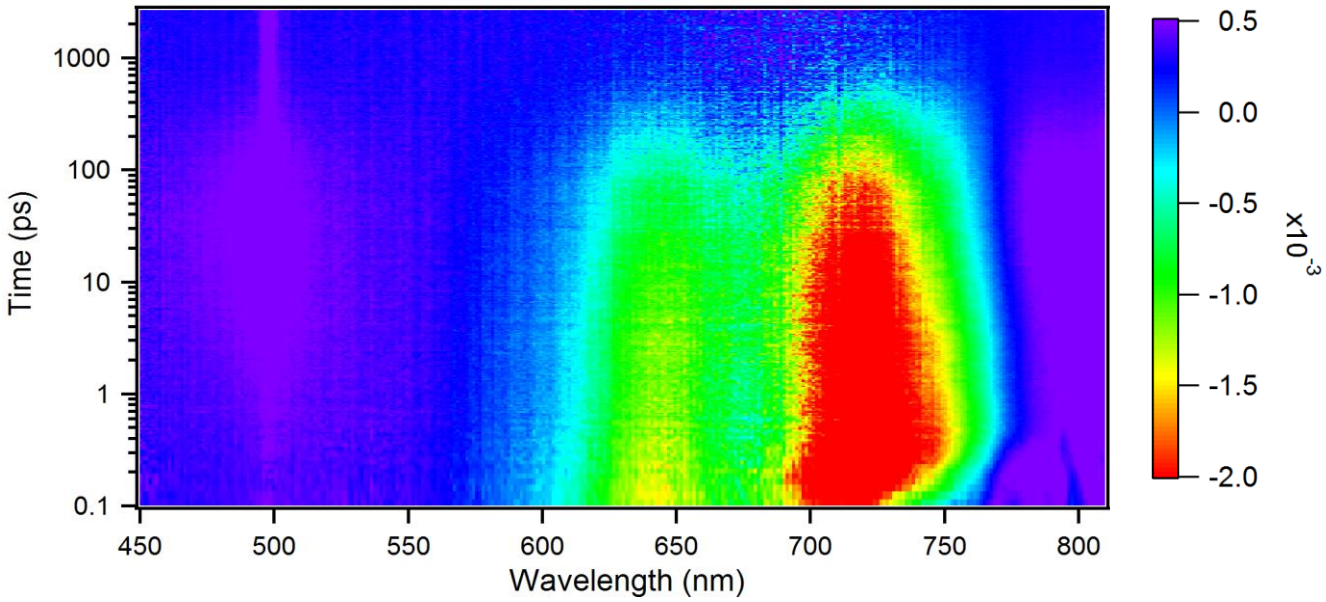

(d) PTB7-Th with 1% ASSQ+1% DPSQ

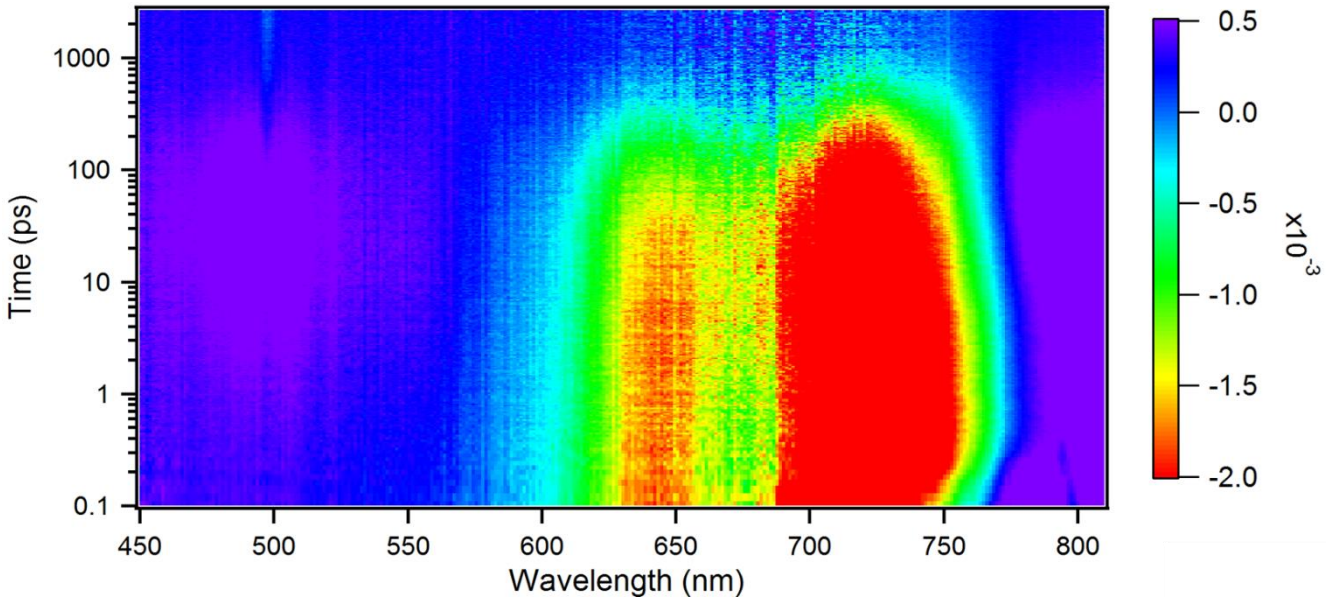

(e) DPSQ (neat film), excited at 500 nm

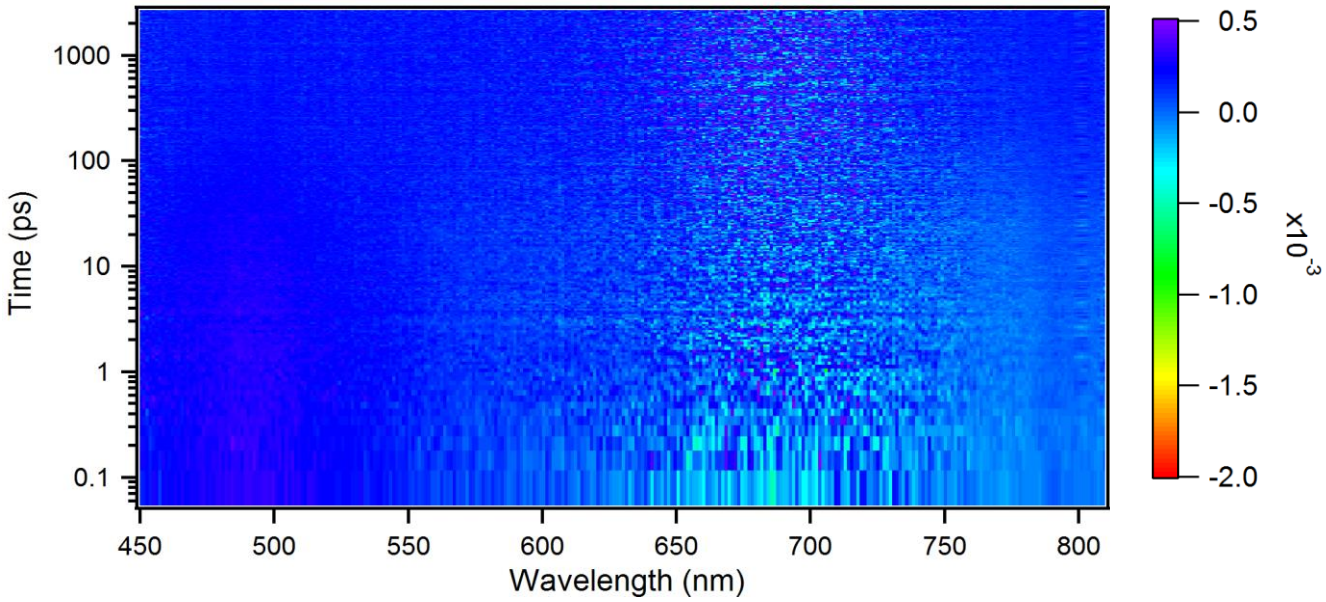

Ultrafast transient absorption experiments were conducted on films excited at 500 nm and laser fluence was set below 10 μJ cm^{-2}, to ensure linear response of the TA signals from ASSQ, PTB7, PTB7-Th, and PT8. Color bars of the TA contour plots shows absorption signal changes in optical density unit. We show a negative signal (red region) containing two peaks at 560 and 620 nm, which corresponds to the PT8 absorption (or GSB) with 0–1 and 0–0 vibrational transitions, respectively (Fig 3e). Introducing DPSQ into PT8 causes a negative TA signal at 740 nm (Fig. 3d), accompanying with a mitigated GSB of PT8. In both cases for PTB7-DPSQ and PT8-DPSQ, we observe the photoinduced absorption of the polarons at 490 nm associated to DPSQ, inferring rapid excitation energy transfer from the polymer to the dye molecule.

TA experiments on neat DPSQ film was performed to verify that the GSB of DPSQ cannot be triggered by 500 nm excitation source per se, even with higher fluence at ~ 20 uJ cm^{-2}. The results shown in S2e is rather weak compared to the strong GSB signal of DPSQ as demonstrated in figures 2d, 2k, and 2l.

S3 GIWAXS data

S3a GIWAXS: Ternary blends of (a) 2% ASSQ and (b) 2% DPSQ in PTB7:$PC_{71}BM$ films under the same color scale. The data is further extracted and plotted as (c) in-plane and (d) out-of-plane line-cuts.

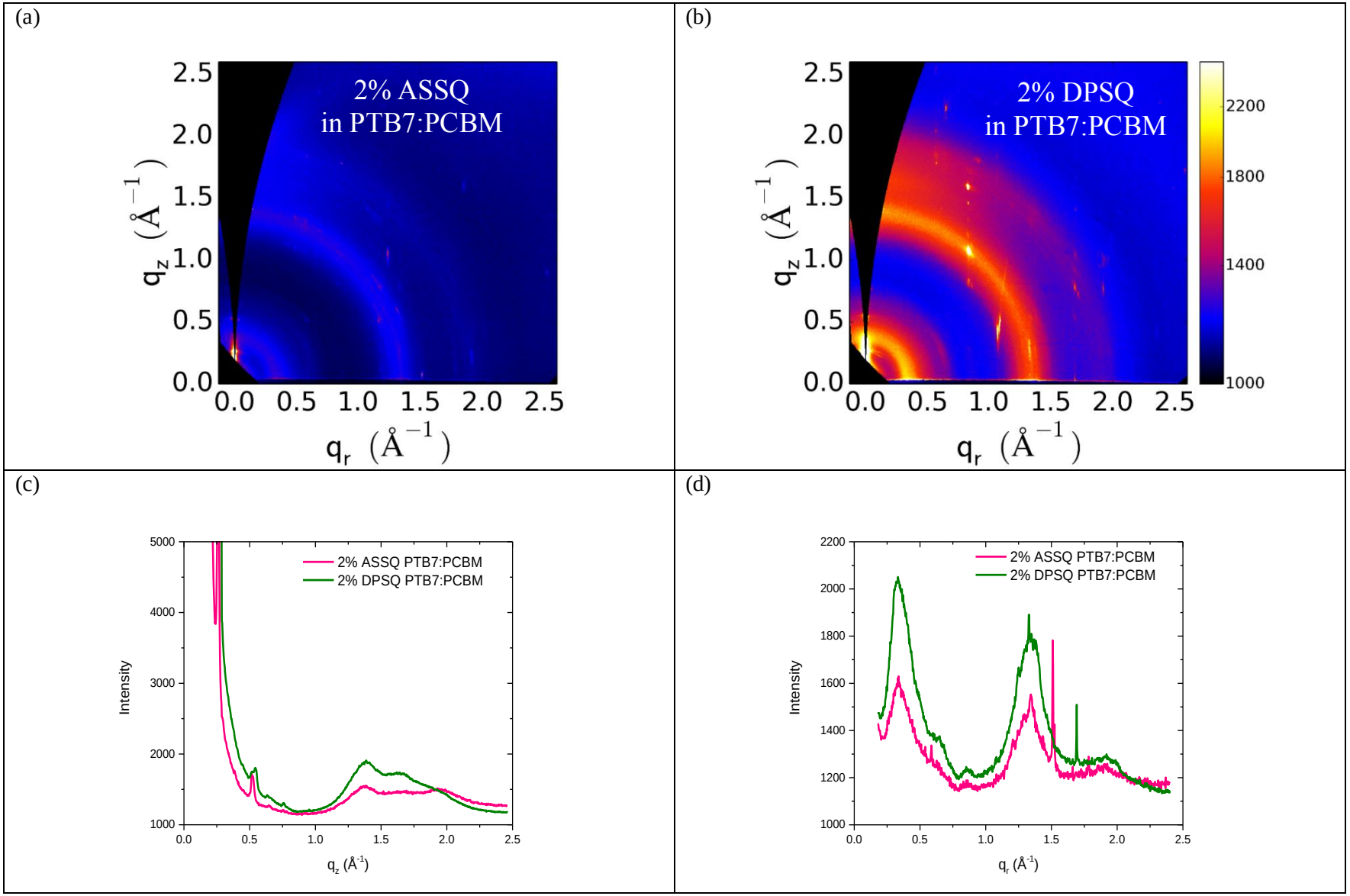

S3b GIWAXS: (a) Binary PTB8:$PC_{61}BM$ and (b) quaternary ASSQ:DPSQ:PT8:PCBM scattering patterns with the same color scale are plotted as (c) in-place and (d) out-of-plane linecuts

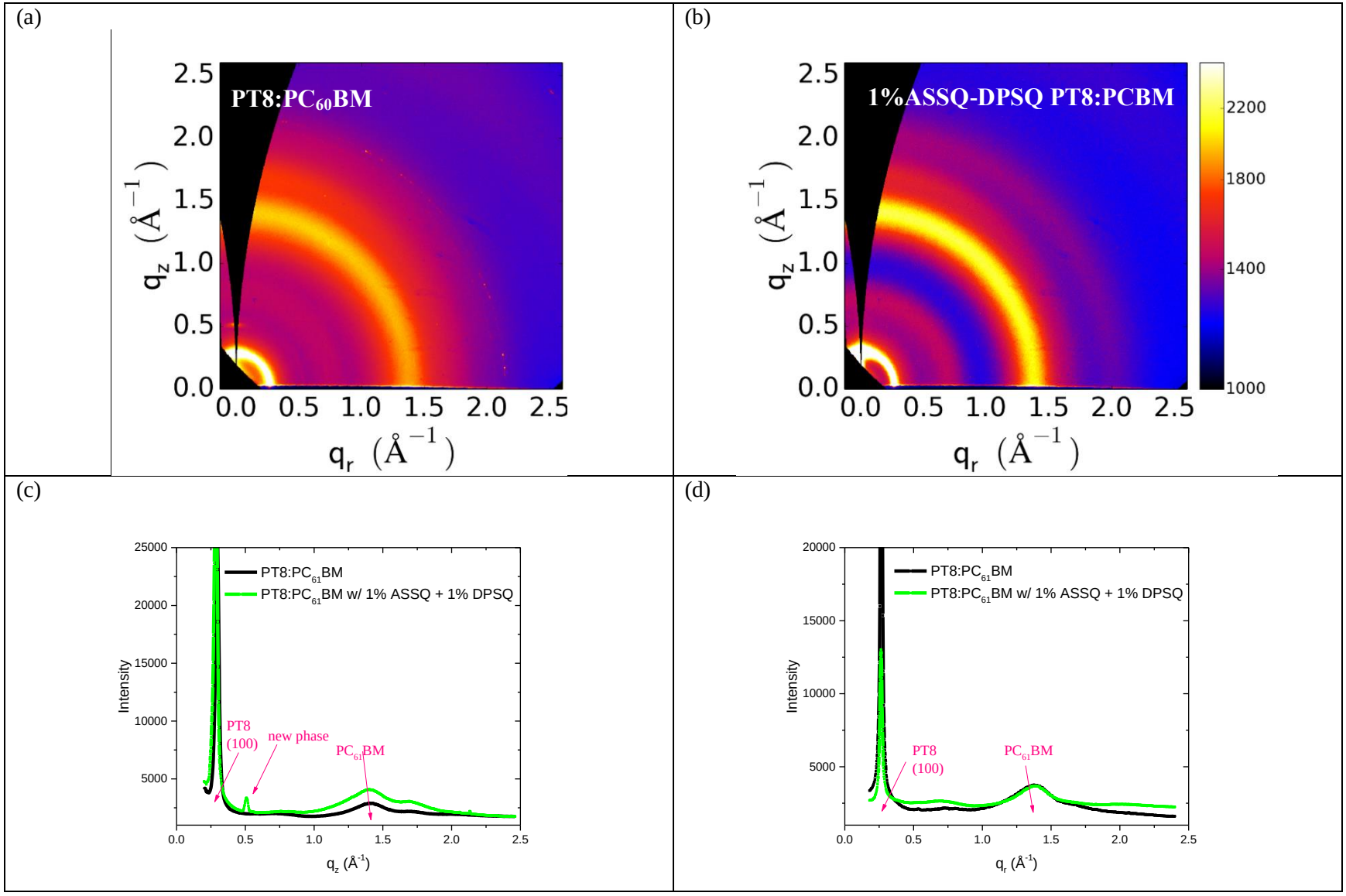

Note: For PT8 systems, we observe co-crystalline phase in the quaternary blend as well. However, the changes are not as intense as in the case of PTB7 as host polymer (Fig. 5f, g). Differences in polymer:fullerene ratio, processing solvents, polydispersity index, molecular weight of the polymer and polymer substituents are some of the factors that we propose could alter the magnitude of co-crystalline phase formation.

S3d Fitting data of out-of-plane linecut of 1% ASSQ-DPSQ PTB7:$PC_{71}BM$

Peak Analysis

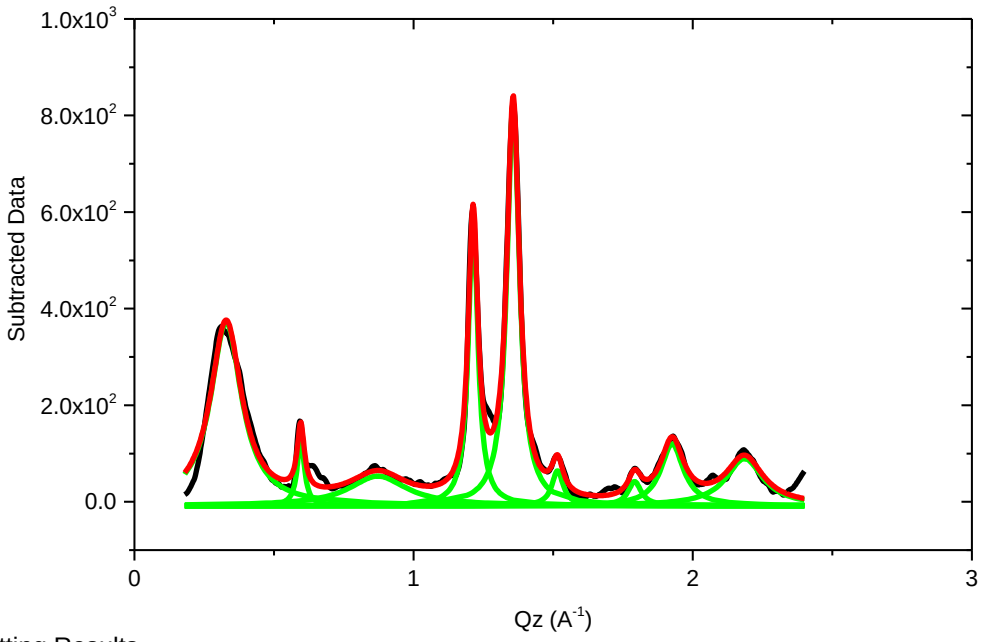

Fitting Results

Peak Index	Center Max	Area Intg	FWHM	Max Height	Area Intg	Area IntgP
1.	0.32841	68.90016	0.13527	379.93649	68.90016	27.00911
2.	0.59593	6.5639	0.03077	137.78192	6.5639	2.57307
3.	1.2133	37.76397	0.04158	585.1453	37.76397	14.80361
4.	1.35684	69.25482	0.05402	829.10844	69.25482	27.14814
5.	0.87205	22.18651	0.25105	61.3669	22.18651	8.69719
6.	1.51557	5.53203	0.04937	72.39744	5.53203	2.16857
7.	1.79189	4.41879	0.0575	49.95693	4.41879	1.73218
8.	1.92629	18.95225	0.09848	127.88072	18.95225	7.42935
9.	2.18556	21.52728	0.16054	97.75485	21.52728	8.43877

S3e Summary of domain orientation percentage on binary and quaternary films

PTB7 100 (lamellar) peak analysis at 0.39 Å^{-1}

Material	theta (degrees)	iso	q_r	q_z	total	isotropic	face-on	edge-on
Binary	0.07	1795	637	9211	11643	15%	5%	79%
Binary	0.10	7994	9495	11632	29122	27%	33%	40%
Binary	0.12	3929	7378	8792	20100	20%	37%	44%
Binary	0.15	4792	1901	4942	11636	41%	16%	42%
Binary	0.20	4834	1153	3807	9795	49%	12%	39%
Quaternary	0.07	5705	2957	4383	13046	44%	23%	34%
Quaternary	0.10	7271	5912	5515	18698	39%	32%	29%
Quaternary	0.12	5517	5310	5062	15890	35%	33%	32%
Quaternary	0.15	2937	2997	3331	9266	32%	32%	36%
Quaternary	0.20	3267	1680	2097	7045	46%	24%	30%

New unique phase in quaternary films: "Co-crystal" peak at 0.277 Å^{-1}

Material	theta (degrees)	iso	q_r	q_z	total	isotropic	face-on	edge-on	conclusion
Binary						0%	0%	0%	Peak not present (no co-crystal)
Quaternary	0.07	0	0	178852	178852	0%	0%	100%	Co-crystal is entirely edge-on
	0.10	0	0	147793	147793	0%	0%	100%	
	0.12	0	0	112445	112445	0%	0%	100%	
	0.15	0	0	76875	76875	0%	0%	100%	
	0.20	0	0	63999	63999	0%	0%	100%	

In these tables, ‘theta’ refers to the incident beam angle with respect to the sample surface plane. Data displayed in Figure 5 are results of theta = 0.12.

S3f Description on the quantification of crystallite population analysis on GIWAXS data

Quantification of semiconducting polymer orientation was performed using a previously-described procedure[2]. The intensity along the 100 lamellar arc was integrated at each angle (χ) with respect to the q_z axis[3, 4]. The full peak width was integrated, and the local background, just outside the peak region subtracted, at each angle. The χ scale was corrected to account for the intersection of the Ewald sphere[5]. To account for the amount of material being probed at any given angle, assuming films were in-plane powders, we apply a sin(χ) correction factor[6]. To compute the amount of face-on vs. edge-on material, we distributed the integrated intensity of the corrected curve into three categories: "isotropic" (baseline scattering that is uniform in the uncorrected curve, and follows sin(χ) in the corrected curve), "edge-on" (signal above baseline for χ < 45º), and "face-on" (signal above baseline for χ > 45º).

S4. Hole mobility comparison for binary, ternary, and quaternary devices

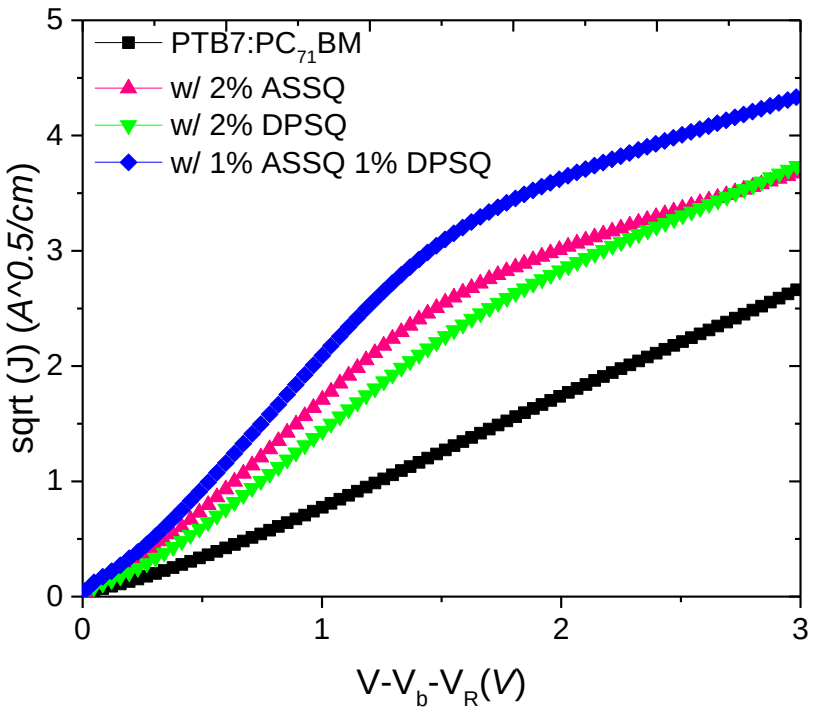

Active layer	**Linear slope, (r^2 = 0.9998)** ($A^{0.5}V^{-1}cm^{-1}$)	$\mu_{0,h}$* ($cm^{-2}V^{-1}\cdot s$)	***L*** (nm)
PTB7:PC_{71}BM Control	0.9243	6.281×10^{-4}	130
2% DPSQ mixed	1.587	1.122×10^{-3}	110
2% ASSQ mixed	1.831	1.938×10^{-3}	120
1% ASSQ-DPSQ mixed	2.147	2.666×10^{-3}	120

Zero-field hole mobility is estimated by space-charge limited current model (SCLC) under low applied voltage where the anode is grounded. Devices studied were constructed as ITO/MoO_3/Active layer/MoO_3/Au. Device area was kept consistent with solar cells (8 mm^2). Thickness is estimated by cross-section scanning electron microscope imaging after the J-V characteristics under dark conditions were tested. Data was fitted to the Mott-Gurney equation below, where voltage is corrected to voltage applied minus the bias voltage (ground) and resistive voltage. Resistive voltage accounts for loss due to resistance in ITO (20 Ω). L denotes the film thickness and the epsilons correspond to vacuum and relative permittivities.

$$J = \frac{9}{8}\varepsilon_0\varepsilon_r\mu_0\frac{(V - V_b - V_{IR})^2}{L^3} \qquad (3)$$

S5. X-ray Photoelectron Spectroscopy (XPS)

S5a. Surface element quantification for binary and quaternary films. Scattered dots in the element analysis of C 1s and S2p are raw data and the lines are fitted results.

PTB7:PCBM	with 2% ASSQ+DPSQ
Full spectra 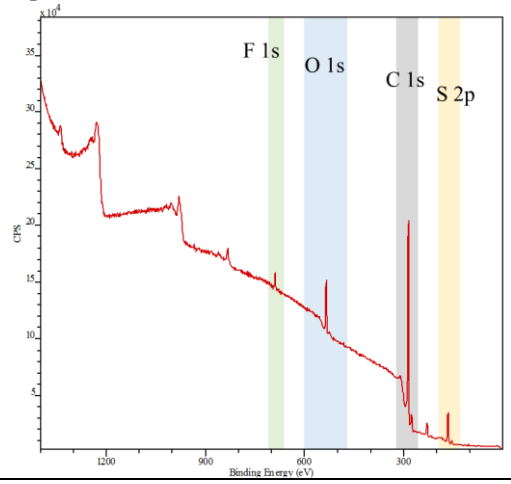	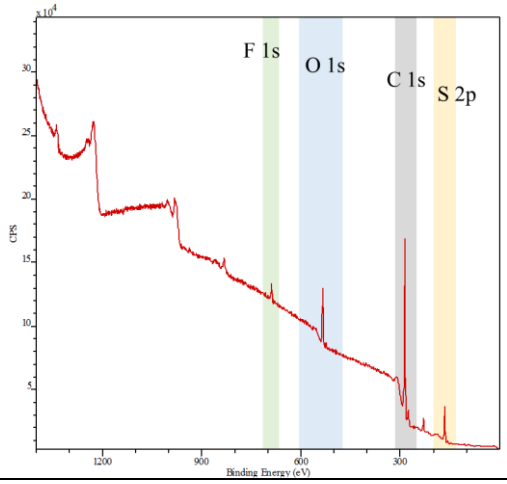
C 1s 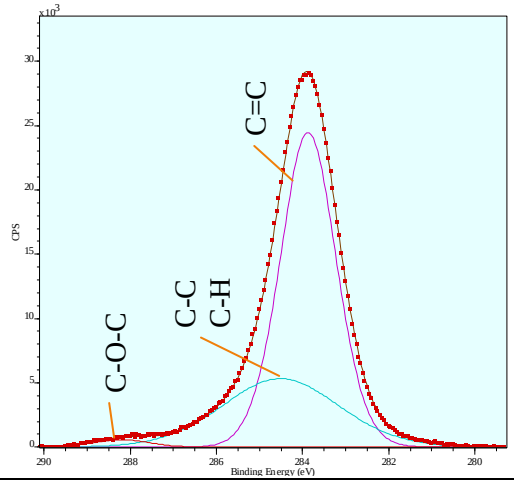	C 1s 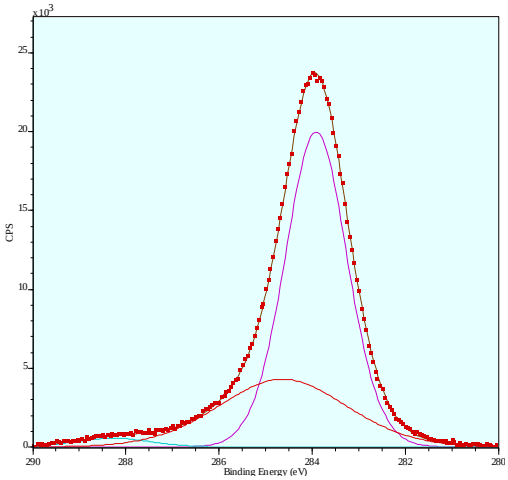
S 2p 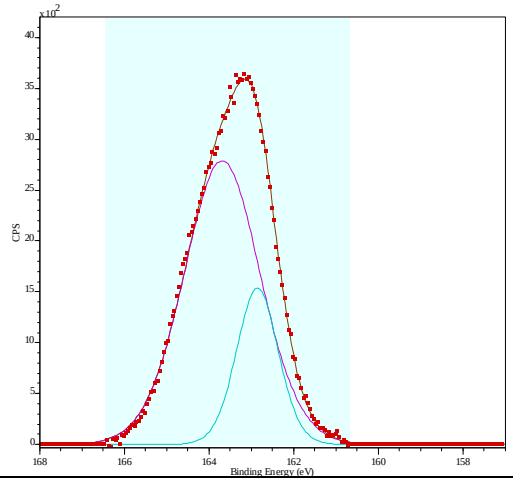	S 2p 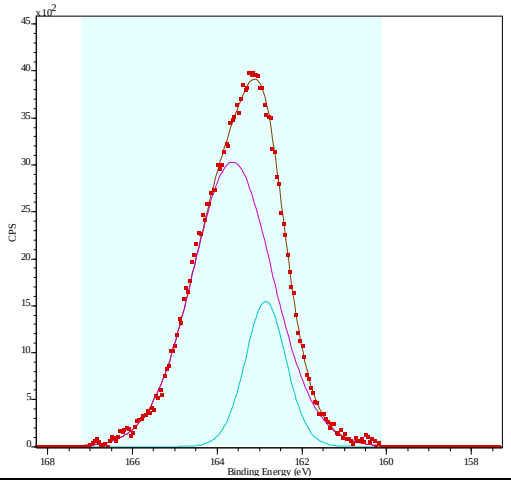

Table S1: Quantification of carbon and sulfur of binary and quarternary films

	PTB7:PCBM		**with 1%ASSQ+DPSQ**	
Peak	**C 1s**	**S 2p**	**C 1s**	**S 2p**
Area under Peak	16525.7	2395	13906.1	2677.6
FWHM	1.696	2.195	1.751	2.247
Max Height	29105.1	3645.5	23699.6	3980
R.S.F.	1	1.68	1	1.68
Area/RSF	16525.7	1425.6	13906.1	1593.8
Ratio (C:S)	0.9206	0.0794	0.8972	0.1028

As a surface sensitive analytical tool, X-ray photoelectron spectroscopy (XPS) was used to survey element distribution at the top interface. For the dual-squaraine PTB7:$PC_{71}BM$ system, we correlate the XPS data to morphological change by quantifying the carbon to sulfur ratio on the surface, as sulfur is only present in the thiophenyl backbone of PTB7 (*Supplementary Information, S5*). Close scanning of the carbon 1s peak at 280 to 290 eV binding energy reveals a shoulder at 288 eV which corresponds to the presence of C-O bonding in PCBM[7] and a strong characteristic peak of C=C from the conjugated organics at 284 eV. By integrating the area under the carbon 1s and sulfur 2p spectra (peak at 163.4 eV) and normalizing to their relative sensitivity factors, we notice that the S:C ratio increases from 0.08:0.92 to 0.10:0.9 after ASSQ and DPSQ were mixed in the polymer:fullerene matrix. Because only the polymer contains sulfur element, this indicates that the squaraines promote a more polymer-rich surface formation, resulting in a better concentration gradient for charge extraction near the cathode interface[8, 9] for inverted solar cells. We attempted to quantify the percentage of squaraines on the surface by repetitively scanning the region from 395 to 408 eV binding energy, but the signal from the nitrogen 1s is not discernable (*Supplementary Information, S5b*) in 2% ASSQ-DPSQ PTB7:$PC_{71}BM$ film. The nitrogen 1s peak, however, is clearly seen in 1:1 blended ASSQ-DPSQ film. Hence, we deduce that squaraines are indeed present in trace amount on the film surface.

S5b. Detailed XPS scans for N 1s on 1% ASSQ + 1% DPSQ PTB7:$PC_{71}BM$ films

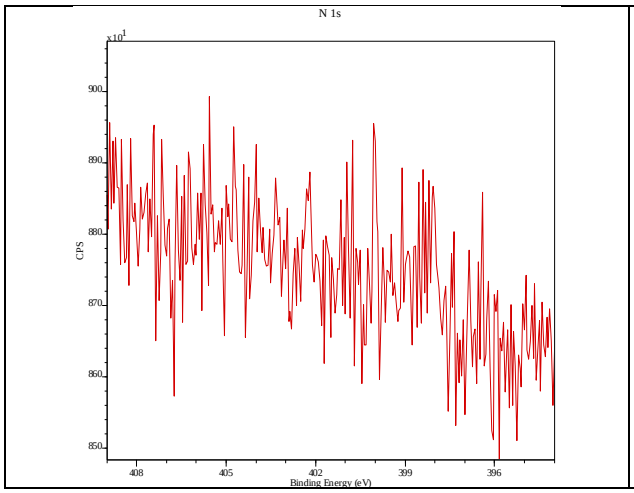

- Nitrogen 1s peak is not spotted in 1%ASSQ-DPSQ PTB7:$PC_{71}BM$ film even after 20 continuous scans.

S5c. XPS spectra on 1:1 ASSQ:DPSQ films: (a) XPS full spectrum scan for equi-mass of ASSQ:DPSQ blended film (b) Nitrogen 1s peak shown in ASSQ:DPSQ squaraines film.

(a)

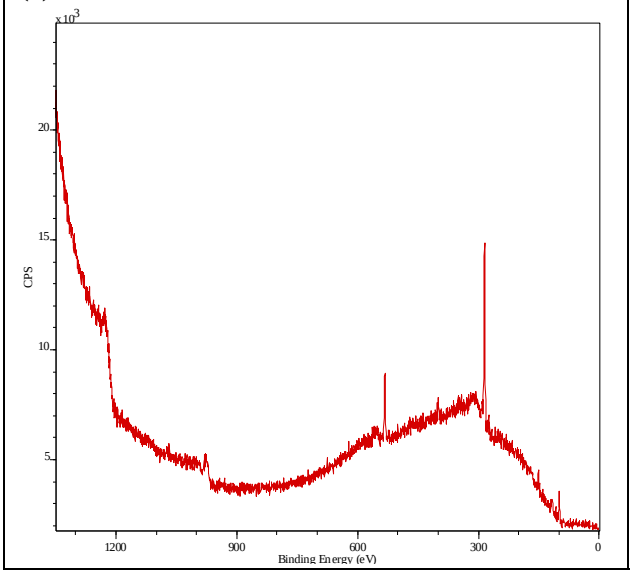

(b)

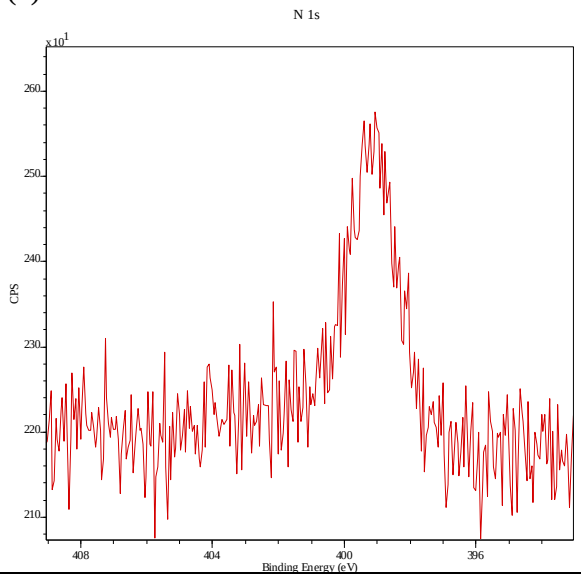

S6 X-SEM and TEM images

S6a Cross section SEM images (X-SEM) in false colors for binary and quaternary cells on ITO (or glass portion of ITO substrates). Films were rapidly cooled in liquid nitrogen before cleavage.

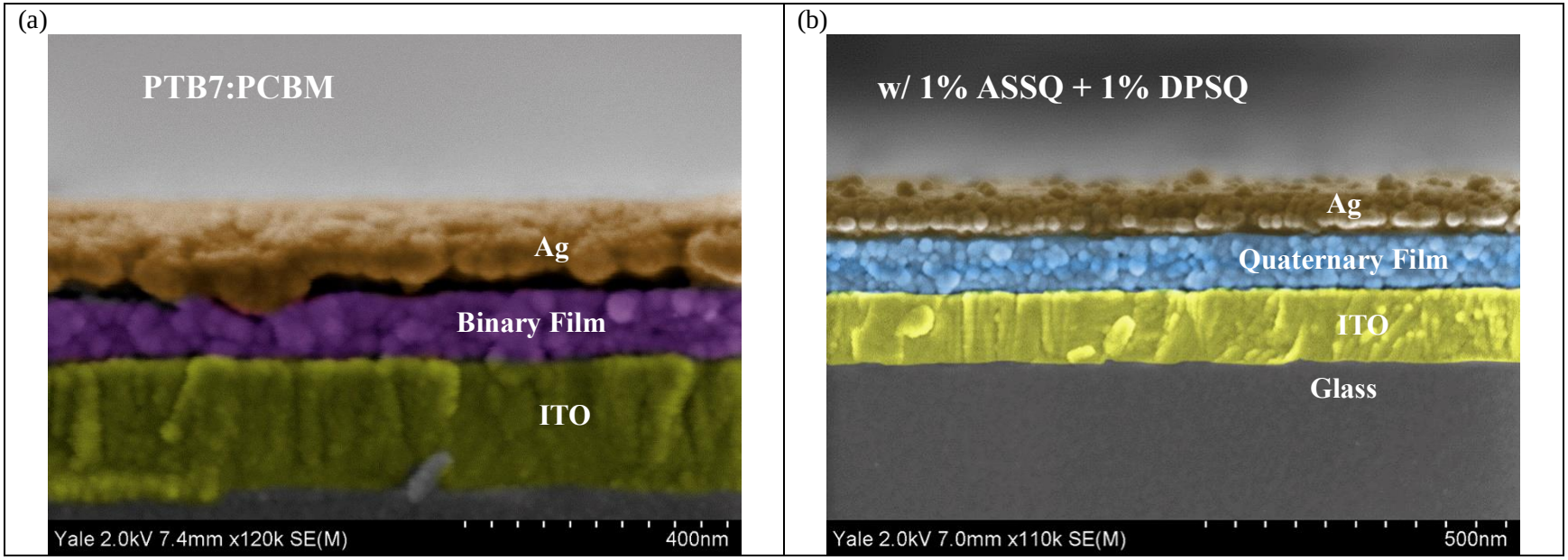

X-SEM results were used to estimate the thickness of the active layers of the PTB7:$PC_{71}BM$ films. Adding squaraines has little effect on the film thickness and hence the solar cells performance improvement is not associated with the light absorbing thickness. In this case, both binary and quaternary films share thickness of ~ 94 nm.

S6b TEM: EDAX of 1% ASSQ-DPSQ PTB7:$PC_{71}BM$

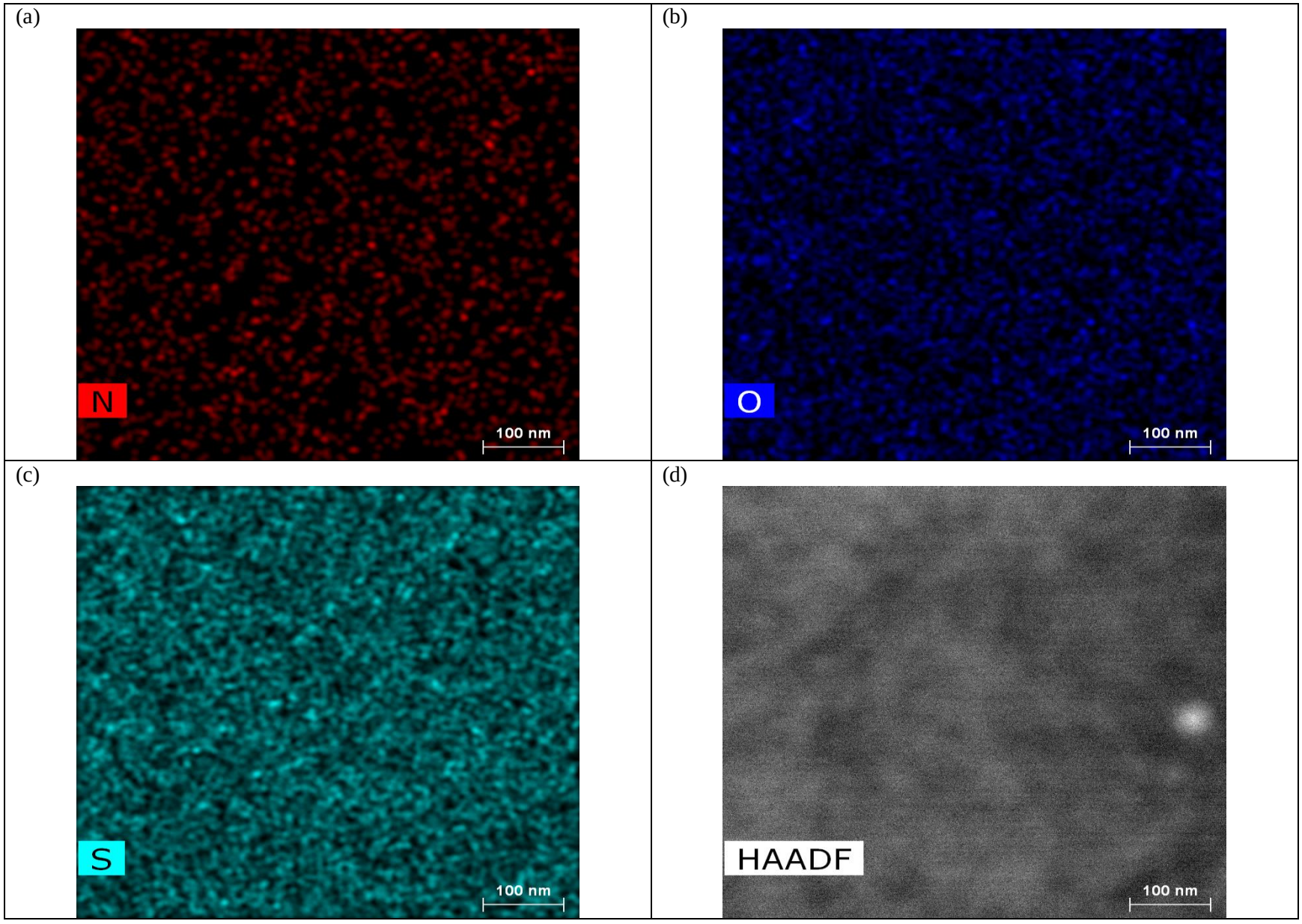

S6c TEM: EDAX of 1% ASSQ-DPSQ PT8:$PC_{61}BM$

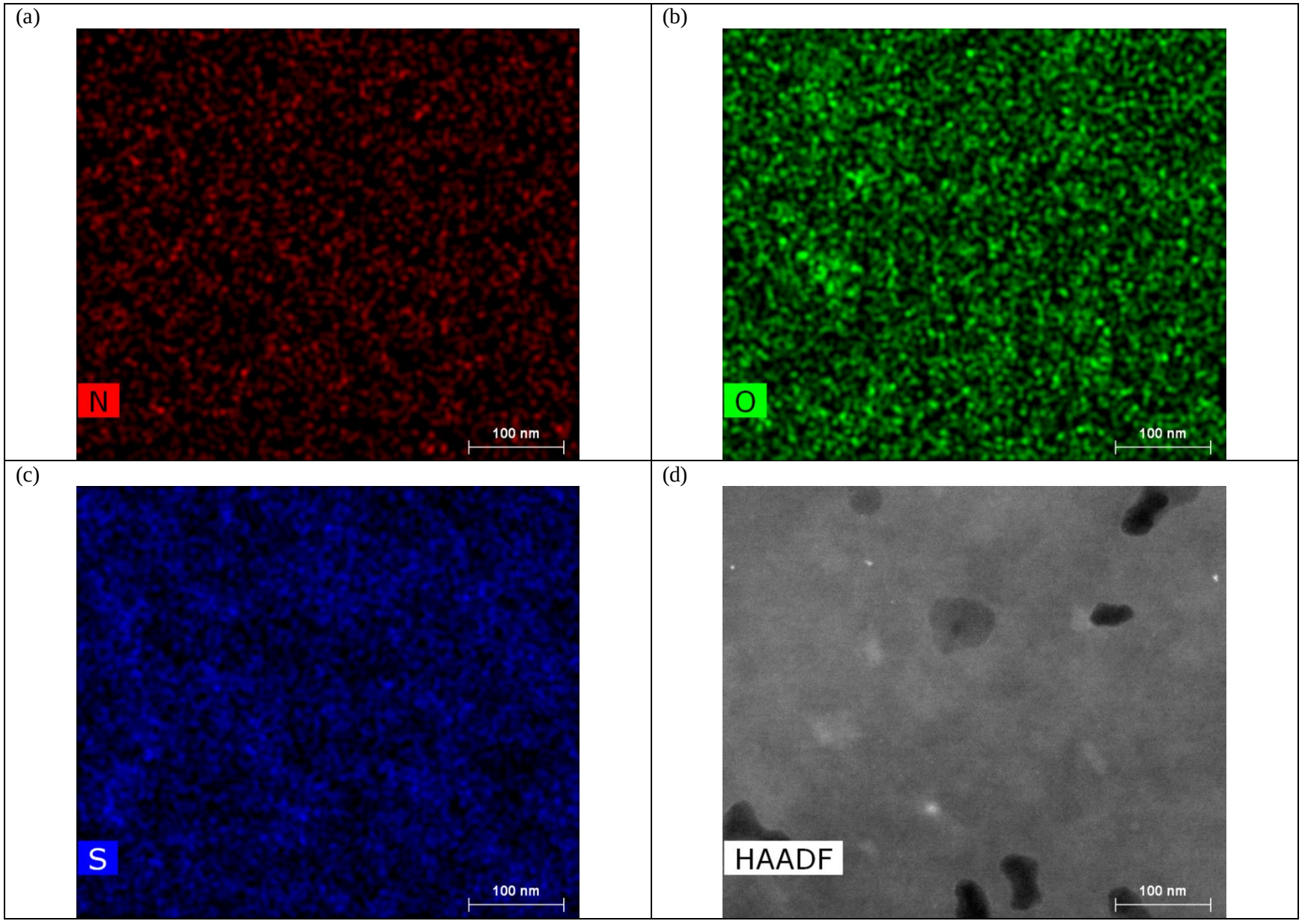

S7 Solar cell performance of Ternary Solar Cells, (a, c) 2% ASSQ and (b, d) 2% DPSQ in PTB7:$PC_{71}BM$ under 1 sun irradiation (a, b) and various illumination intensity (c, d). The EQE difference of ternary devices compared to the control cell without squaraine can be derived from Figure 4(b). This information shows in detail the contribution when only (e) 2% of ASSQ and (f) 2% of DPSQ were added to the control PTB7:$PC_{71}BM$ active layer.

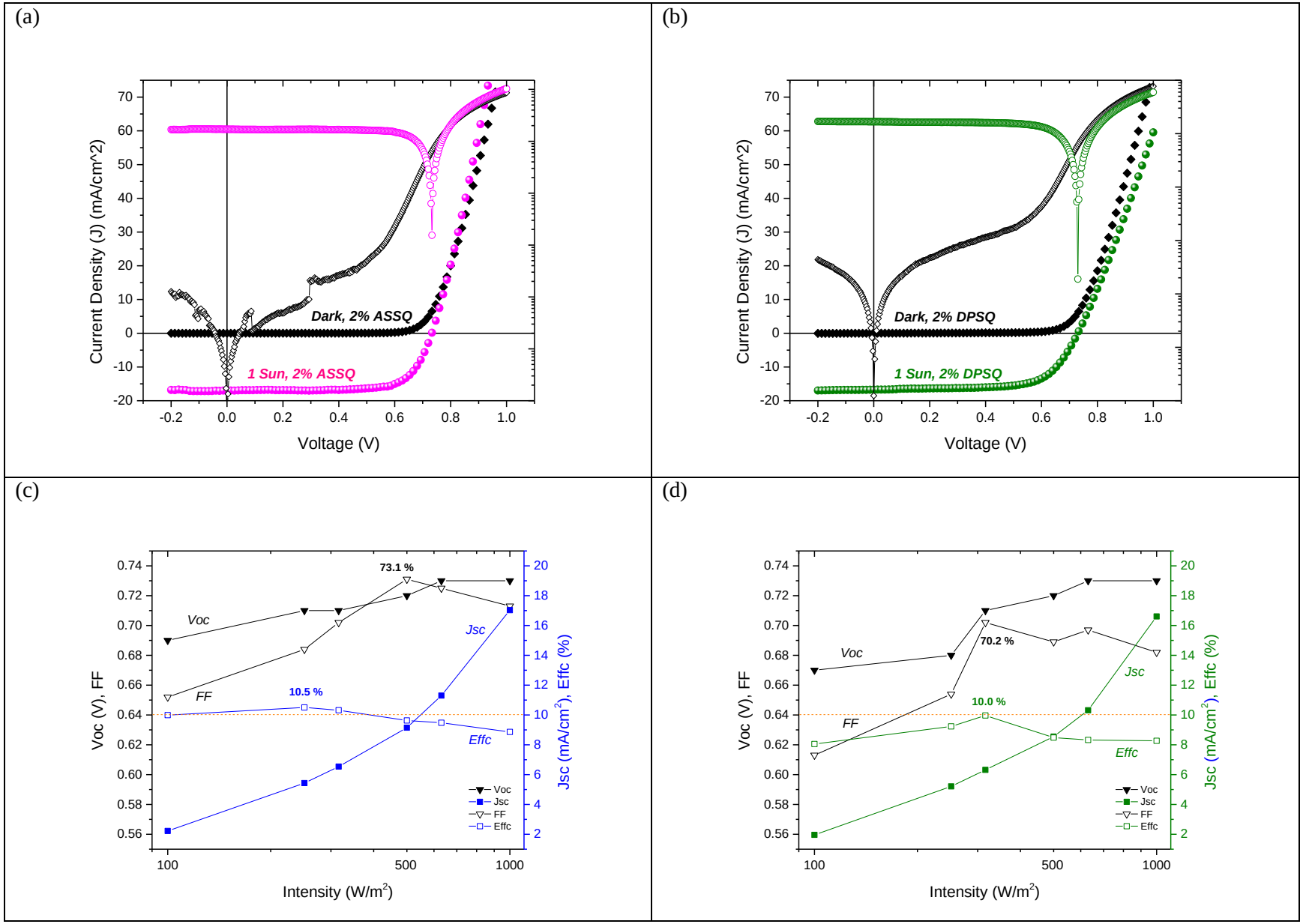

(e)

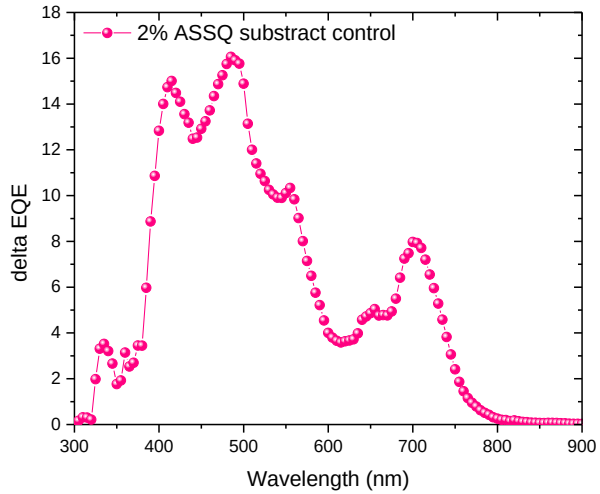
2% ASSQ substract control
delta EQE
Wavelength (nm)
0
2
4
6
8
10
12
14
16
18
300
400
500
600
700
800
900

(f)

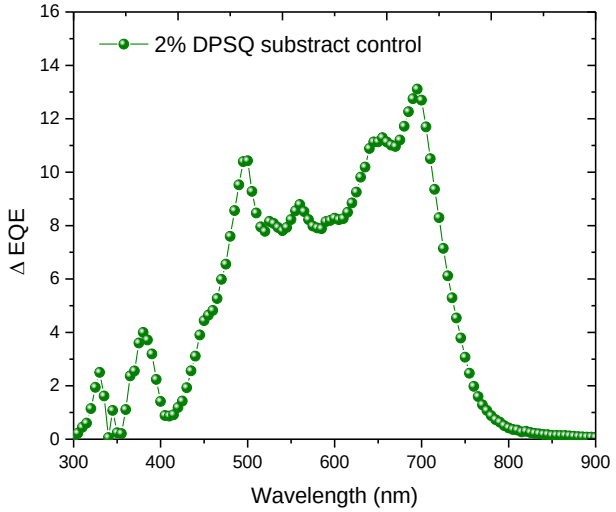
2% DPSQ substract control
Δ EQE
Wavelength (nm)
0
2
4
6
8
10
12
14
16
300
400
500
600
700
800
900

S8 Supplemental solar cell performance of quaternary solar cells using ZnO as interlayer. (a) PCEs of 60 devices of ASSQ:DPSQ:PTB7:$PC_{71}BM$ quaternary films under AM 1.5 1 sun simulated illumination. Dark J-V curves of (b) PTB7:$PC_{71}BM$, (c) PTB7-Th:$PC_{71}BM$, and (d) PT8:$PC_{61}BM$ with their quaternary counterparts. (e) Comparison of EQE difference between quaternary and binary devices of PTB7:$PC_{71}BM$. (f) EQE of binary and quaternary PTB7-Th:$PC_{71}BM$ cells and the inset is the EQE difference.

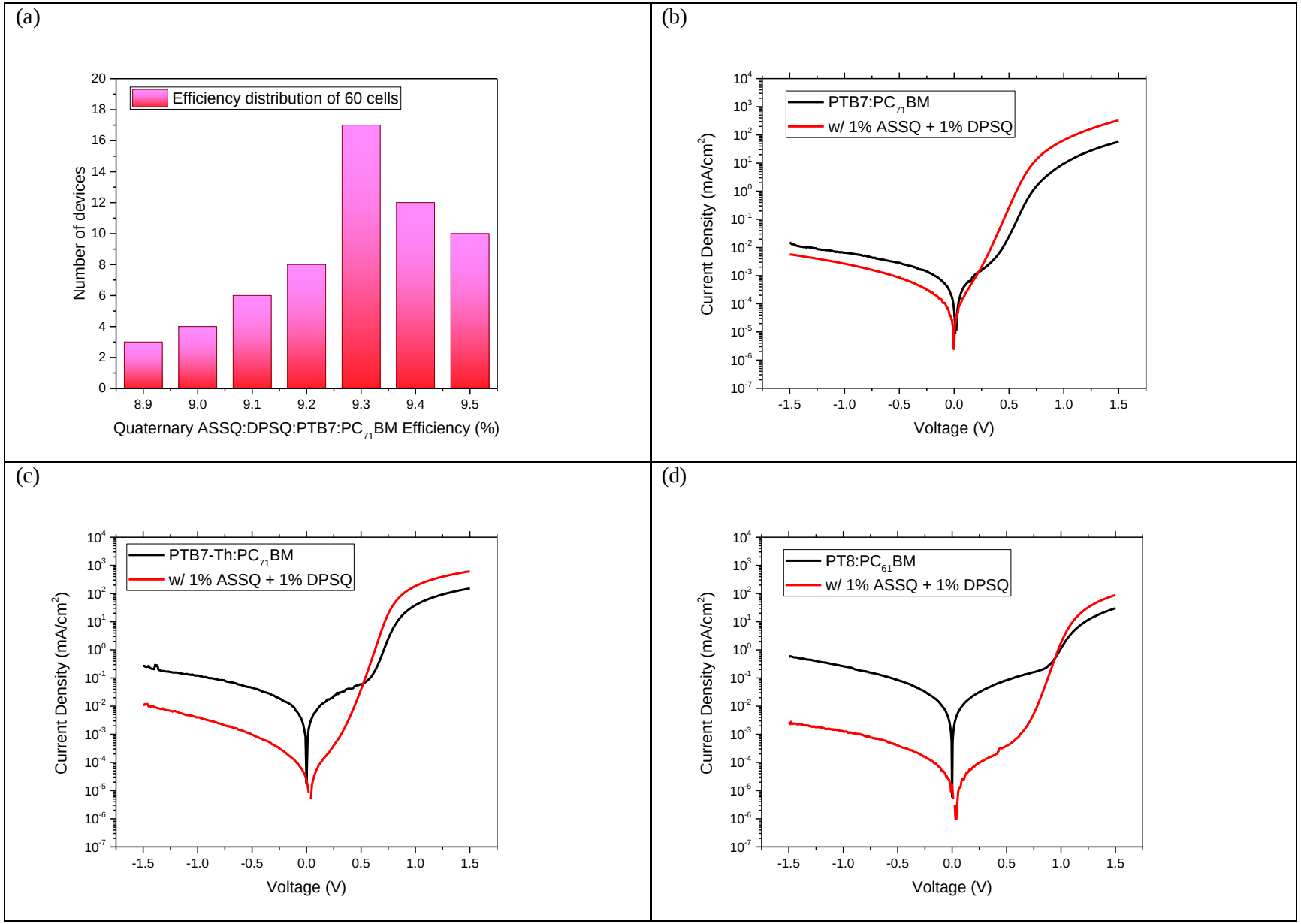

(e)

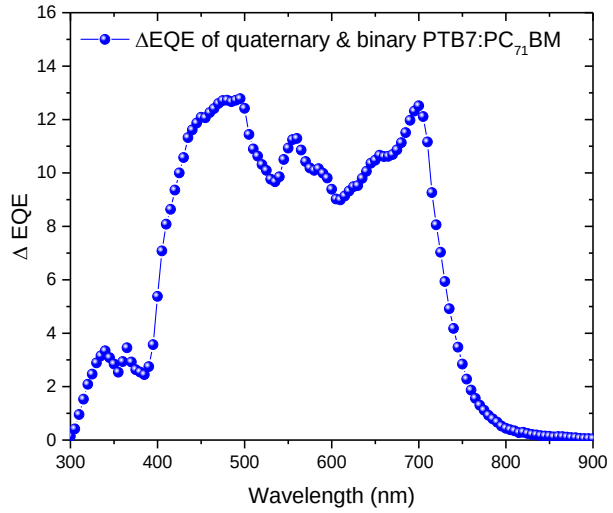
ΔEQE of quaternary & binary PTB7:PC71BM
Δ EQE
Wavelength (nm)

(f)

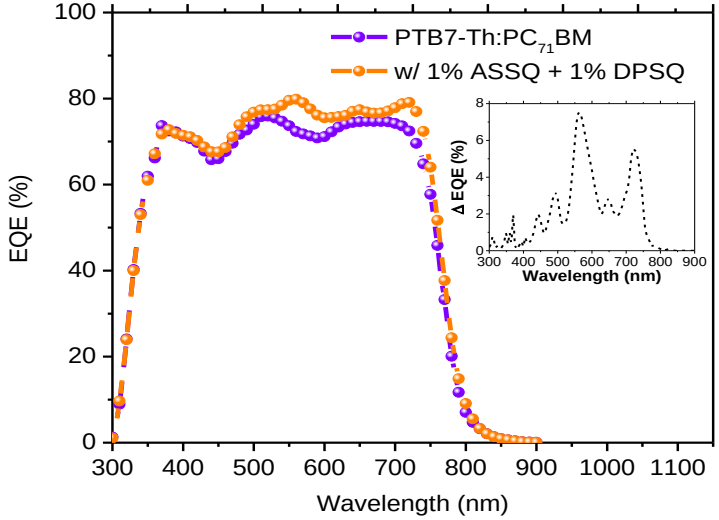
PTB7-Th:PC71BM
w/ 1% ASSQ + 1% DPSQ
EQE (%)
Δ EQE (%)
Wavelength (nm)
Wavelength (nm)

S9 Energy level alignment and device parameter statistics of quaternary systems.

(a) PTB7:$PC_{71}BM$ with ASSQ and DPSQ

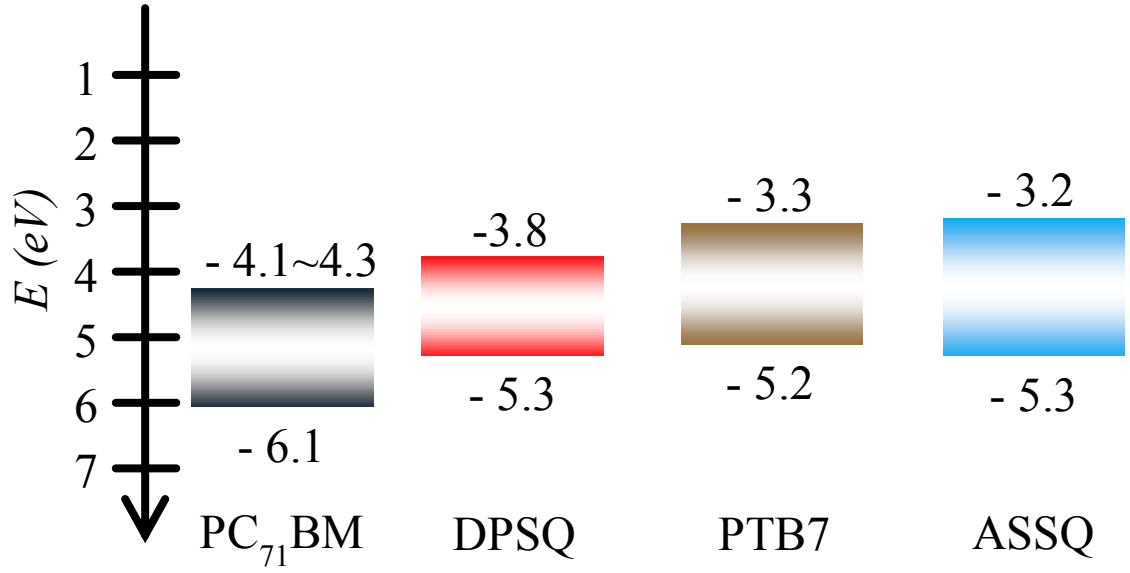

(b) PTB7-Th:$PC_{71}BM$ with ASSQ and DPSQ

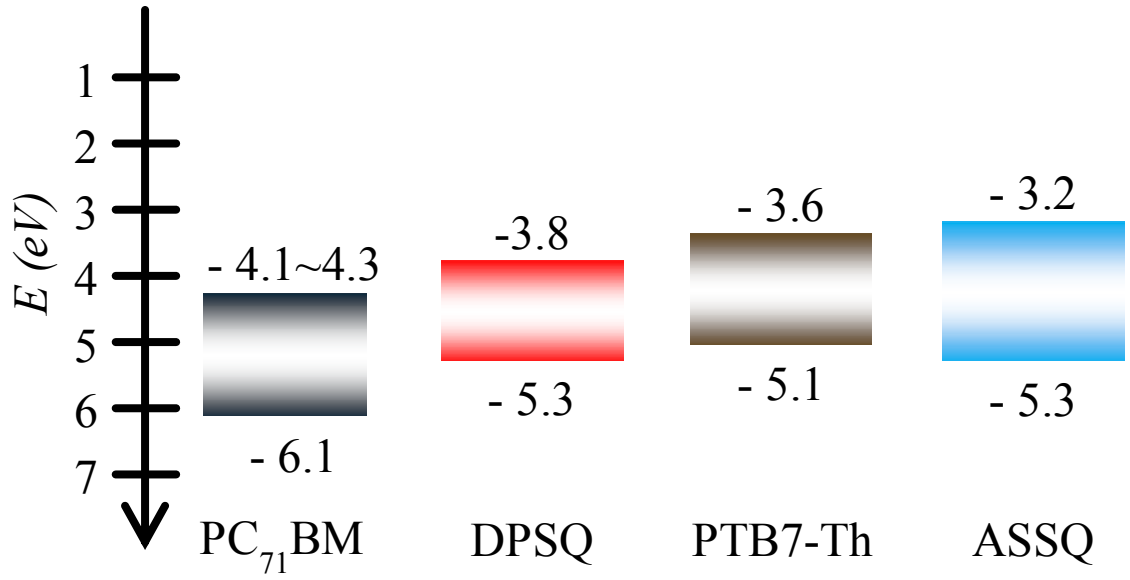

(c) PT8:$PC_{61}BM$ with ASSQ and DPSQ

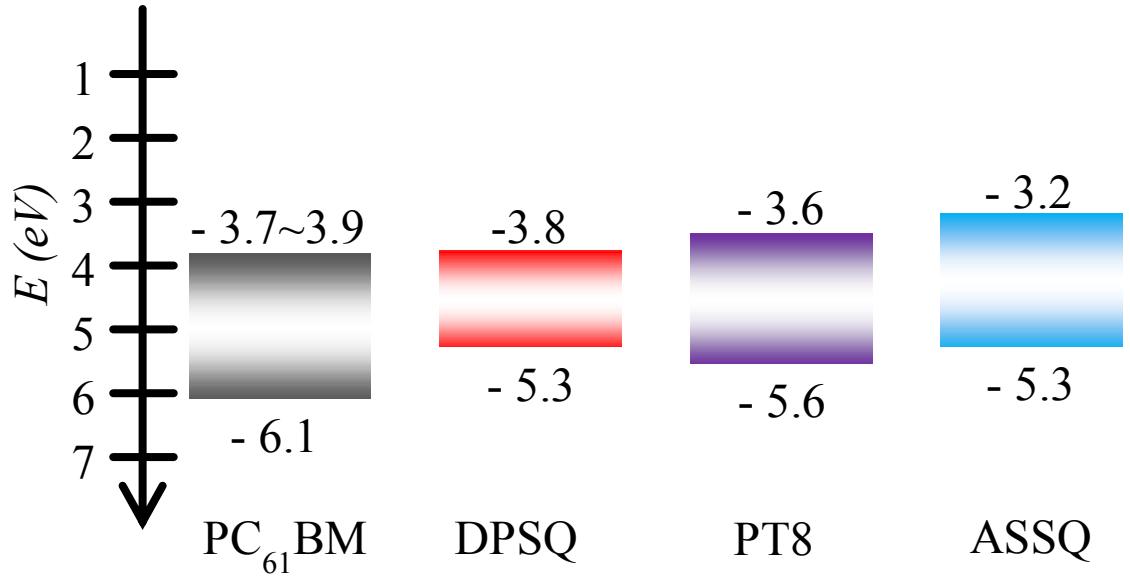

S9(d) Average performance devices of PTB7-Th:ASSQ:DPSQ:$PC_{71}BM$ on PFN

Results presented below are mean and standard deviation values of the best 6 devices with PFN after 15 minutes exposure under simulated 1sun illumination in nitrogen glovebox.

Inverted Devices	Efficiency	Jsc (mA/cm2)	FF (%)	Voc (V)
Binary PTB7:$PC_{71}BM$	8.18 ± 0.16	16.74 ± 0.17	66.3 ± 1.5	0.725 ± 0.01
Ternary 2% ASSQ:PTB7:$PC_{71}BM$	8.83 ± 0.15	17.65 ± 0.17	70.4 ± 0.8	0.721 ± 0.01
Ternary 2% DPSQ:PTB7:$PC_{71}BM$	8.77 ± 0.09	17.73± 0.17	69.9 ± 0.6	0.722 ± 0.01
Quaternary PTB7:$PC_{71}BM$	9.46 ± 0.19	17.88 ± 0.15	71.1 ± 1.2	0.717 ± 0.02
Binary PTB7-Th:$PC_{71}BM$	9.22 ± 0.17	17.05 ± 0.12	68.6 ± 0.9	0.794 ± 0.03
Quaternary PTB7-Th:$PC_{71}BM$	10.45 ± 0.12	17.82 ± 0.16	71.7 ± 1.3	0.789 ± 0.04

Reference

[1] J. R. Lakowicz, *Principles of Fluorescence Spectroscopy*, Springer, New York **2006**.
[2] D. E. Johnston, K. G. Yager, H. Hlaing, X. Lu, B. M. Ocko, C. T. Black, ACS Nano **2014**, 8, 243.
[3] D. E. Johnston, K. G. Yager, C.-Y. Nam, B. M. Ocko, C. T. Black, Nano Lett. **2012**, 12, 4181.
[4] H. Hlaing, X. Lu, T. Hofmann, K. G. Yager, C. T. Black, B. M. Ocko, ACS Nano **2011**, 5, 7532.
[5] J. L. Baker, L. H. Jimison, S. Mannsfeld, S. Volkman, S. Yin, V. Subramanian, A. Salleo, A. P. Alivisatos, M. F. Toney, Langmuir **2010**, 26, 9146.
[6] K. A. Page, A. Kusoglu, C. M. Stafford, S. Kim, R. J. Kline, A. Z. Weber, Nano Lett. **2014**, 14, 2299.
[7] A. B. Belay, Z. Wei, R. Krueger, K. O. Davis, U. Alver, N. Sorloaica-Hickman, IEEE J. Photovolt. **2012**, 2, 148.
[8] G. J. Hedley, A. J. Ward, A. Alekseev, C. T. Howells, E. R. Martins, L. A. Serrano, G. Cooke, A. Ruseckas, I. D. W. Samuel, Nat. Commun. **2013**, 4, 2867.
[9] L. Zhang, X. Xing, L. Zheng, Z. Chen, L. Xiao, B. Qu, Q. Gong, Sci. Rep. **2014**, 4, 5071.